Distortions in Medical Ultrasound Imaging

MAS8091: MMath Project

E. Johns

Supervisor: Dr Nick Parker

Abstract

Medical ultrasound imaging is typically calibrated corresponding to the acoustic velocity of soft tissues, 1540 ms^{-1}. However, acoustic velocities within the body varies and therefore misrepresentation of distances within anatomical structures can arise. Additionally, refraction occurs as ultrasound rays traverse boundaries between dissimilar media. This report presents models that quantify distortions. First the positional distortion of a single dot is considered, forming the foundation for further models based on the distortion of dots which comprise the boundary of circular objects. Finally models of distortions of a simplified foetal head are presented; chosen for its importance in clinical monitoring. The acoustic velocity and the width of the foetal skull are not known and are approximated. The models infer that distortion occurs at varying degrees for sequential boundaries. Furthermore varying the parameters of the foetal skull suggest the acoustic velocity effects the distortions to the greatest extent.

Acknowledgements

Firstly I would like to thank my supervisor, Dr Nick Parker, for his encouragement and patience during the production of this report. I would also like to thank Emma Jones and Hayley Moore for their technical expertise and unwavering support throughout the academic year. Finally, I would like to thank Anna Farrell, Vicki Buchanan and Amanda Thomas for their valuable time and assistance.

Contents

1 Introduction

Ultrasound (US) imaging is commonplace within the practice of medical diagnostics. An ultrasound imaging device consists of two main parts; a transducer and a monitor (shown in Figure 1.1(a)). The transducer both emits and recieves an ultrasound beam and when placed on an area of the body can provide anatomical information on the structures within its field of view. Specifically, the transducer is able to detect any echoes - reflections that occur between boundaries of media of different densities - and record the time of detection. This information, along with an assumed acoustic velocity of 1540 ms^{-1} [1] for ultrasound within the human body, can be used to calculate the distances within the structures in the body and form an image on the monitor in 'real-time'.

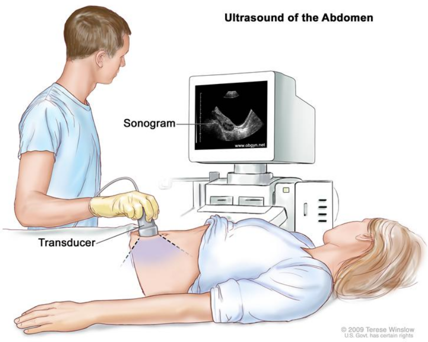

(a)Imaging procedure [2].

(b)US image of a profile of a foetus [3].

Figure 1.1: (a)Pictorial representation of an US image being conducted, (b) B-mode US image of foetus in-vivo.

The concept of ultrasound was discovered in the 1790s by an Italian Catholic priest, biologist and physiologist, Lazzaro Spallanzani [4]. Spallanzani was intrigued as to how bats managed to navigate at night and conducted an experiment in which he hoped to discover their secret. The experiment consisted of two studies, one observing a group of bats that had been blindfolded and the other observing a group of bats that had their ears plugged. He found that, to his surprise, the blindfolded bats managed to manoeuvre around objects effectively, whereas the bats who could no longer hear could not. From this, he concluded that bats must emit a sound, inaudible to the human ear, which they use to judge distances. Unfortunately this idea was met with ridicule and skepticism by the scientific community.

It wasn't until the 1950s that ultrasound imaging was used as a medical diagnostic device by William Nelson [5]. Nelson, or 'Nels' as he was affectionately known, was a modest man who never boasted about his achievements. Even Nelson's own son had no idea of his father's achievements until the day he excitedly told his father of the scan his pregnant wife had undergone. Only then did Nelson reveal his part in the invention to his son.

Today ultrasound images are relied upon to provide accurate information about structures within the body to inform medical decision making. Predominately, clinicians are concerned with the lengths and areas of certain structures. However, most ultrasound images are subject to some degree of distortion [6]. Any area on an ultrasound image which does not accurately represent the anatomical structures present is referred to as an artifact. This report aims to explore some of the possible causes behind these artifacts (Chapter 2) and in particular the distortions that occur in ultrasound images of a foetal head. The main distortions in a cross-sectional image of a foetus' head arise from discrepancies in the real acoustic velocity of media within the skull and the brain, compared to the calibrated velocity of 1540 ms^{-1}.

In Chapters 3-5 models are developed in order to explore and quantify the distortions that occur for a foetal head. Chapter 3 investigates the displacement of the image of a single dot within a medium. Chapter 4 builds upon the principles introduced in Chapter 3 in order to investigate the distortions that occur in circles and ellipses. Finally, Chapter 5 features models which aim to describe the distortions in a foetal head.

2 Principals of Medical Ultrasound Imaging

2.1 Sound and Ultrasound Waves

The ultrasound beam transmitted by the transducer is made up of sound waves. A sound wave is a longitudinal wave and requires a medium in order to travel. The vibrations produced in the medium travel parallel to the wave. Longitudinal waves can be described in terms of sinusoidal plane waves and feature periodic sections of compressions (regions of high density) and rarefactions (regions of low density) [7]. Figure 2.1 is an example of a longitudinal wave and refers to a vibrating string as an analogue of a sound wave.

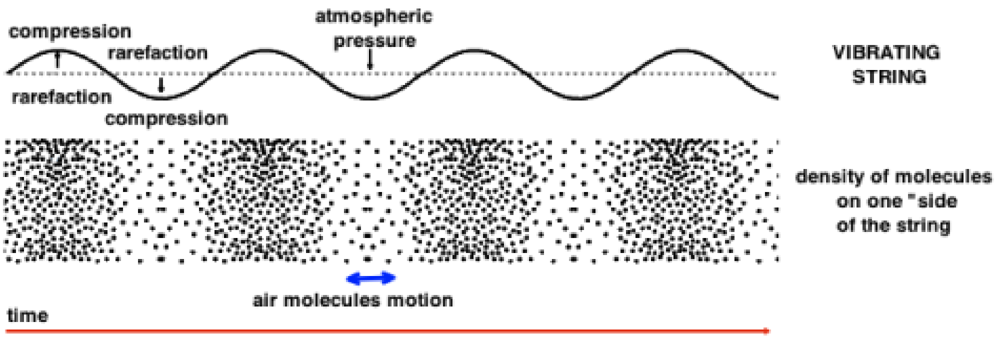

Figure 2.1: Schematic representation of a longitudinal wave [8]

The frequency range of audible sound is 20 to 20,000 Hz. Any sound wave with a higher frequency than this range is classed as ultrasound. Diagnostic ultrasound uses frequencies in the range of 1 to 30 MHz. The frequencies used in medical diagnostics result in relatively short wavelengths when compared to all other sound waves. Short wavelengths produce a higher resolution image but do not penetrate as far into the body. In order to image deeper structures, a larger wavelength is required. Some typical frequency ranges for different parts of the body are [9]:

- Abdominal areas: 3–5 MHz
- Superficial parts*: 5–10 MHz
- Skin or eyes: 10–30 MHz

The wavelength (λ) of a sound wave is inversely proportional to the frequency (f) via the relation,

*On the surface or shallow.

$$\lambda = \frac{v}{f}\,, \tag{2.1}$$

The acoustic velocity within human tissue is approximately 1540 ms^{-1} [10]. For example, the wavelength for a typical abdominal scan from equation (2.1), with $v = 1540$ ms^{-1} and $f = 4$ MHz, is therefore 3.85×10^{-4}m.

2.2 Benefits of using Ultrasound as an Imaging Technique

Currently, ultrasound is one of the most popular imaging techniques in medical diagnostics, second only to x-ray imaging [11]. Ultrasound devices can be portable and are relatively cheap when compared to other imaging modalities, such as Magnetic Resonance Imaging (MRI) and Computer Aided Tomography (CAT) [11]. Also, unlike x-rays, ultrasound imaging does not require the use of radiation, which has inherent health risks [12]. Furthermore, images can be acquired in real-time, a feature which can be exploited to aid intervention procedures and guide some surgeries.

Since US imaging does not require the use of radiation, it is not surprising that this imaging modality is the most commonplace for examining a foetus in-vivo. However US imaging procedures are performed throughout a range of medical specialisms. Abdominal ultrasound scans can be used to image organs such as the liver, gallbladder, kidneys and pancreas. Additionally, ultrasound imaging has a variety of applications within the field of gynecology [13].

2.3 The Ultrasound Imaging Device

Within the core of the transducer there exists a number of piezoelectric crystals [14]. These crystals possess the ability to vibrate and produce sound of a particular frequency when electricity is passed through them. An ultrasound transducer has a particular array type, where an array is the spatial arrangement of transducer elements. These elements are created by slicing a large piezoelectric crystal into smaller unique parts. Each element sits in its own compartment, shielded by any acoustic or electrical interference from neighbouring compartments. It is these elements that are responsible for the production of ultrasound rays, as well as their detection. However each element produces only a single ray, so many elements are required to achieve a high quality image.

There are several modes of US imaging. This report is concerned with images produced through B-mode (brightness mode) imaging and a typical B-mode scan can be seen in Figure 1.1(b). When an ultrasound ray encounters a boundary, a portion of that ray is usually reflected back towards the transducer, which also acts as a receiver for the reflected rays. Reflected rays are referred to as echoes and it is the production and detection of these echoes that form the basis of ultrasound imaging. The method to calculate the distance of the boundary the ray encountered from the transducer is based upon the simple equation,

$$D = ct\,,$$

where t is the flight time of the echo, c is the assumed acoustic velocity of the medium and D is the estimate of the distance between the transducer and the boundary.

B-mode imaging provides a 2D presentation of echo-producing interfaces in a single plane, with the interfaces portrayed by bright regions [15] . The intensity of the echo is represented by the brightness of the region and the position of the echo is determined from the position of the transducer and the transit time of the acoustical pulse. On an ultrasound image the depth is represented by the vertical axis (y-axis).

2.3.1 Transducer Array Types

There are many array types. Three of the most commonplace within diagnostic medicine are the linear sequential, linear phased and curved sequential arrays [14].

Linear Sequential Array

Transducers which use the linear sequential array are flat and relatively large, typically around 40mm long. The elements are arranged along the edge of the transducer in such a way that the rays they produce are parallel to each other and are all emitted sequentially (Figure 2.2). The resulting image is rectangular in shape with a width equal to that of the size of the transducer.

In order to image a large area, the transducer would have to be at least the same size. This is impractical and expensive to do in practice, so the linear sequential array is reserved for imaging smaller structures which require a high-resolution image. Furthermore, as the transducer edge is flat, if the surface which the transducer is placed upon is curved, artifacts can be produced. This is caused by rays passing through the air in the gap between the transducer and the surface.

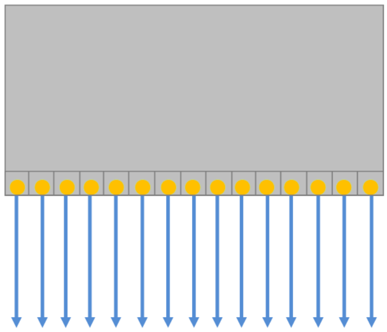

Figure 2.2: Schematic diagram: element arrangement of a linear sequential array. Elements (yellow circles) emit US rays (blue arrows).

Linear Phased Array

The elements in the linear phased array are arranged in the same way as the linear sequential array (shown in Figure 2.3). However, the size of the transducer is much smaller. Each element within the transducer can be excited simultaneously, whilst applying different delays to each element. This creates many individual waves which constructively interfere.

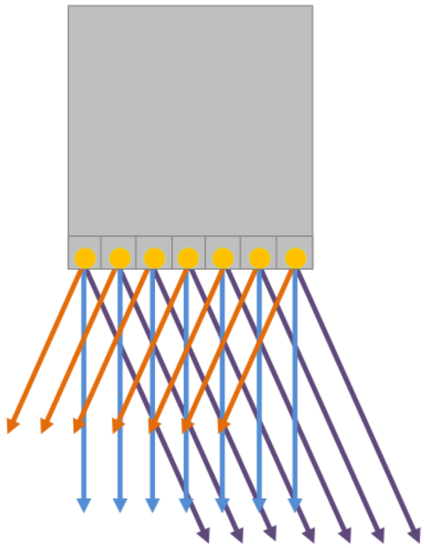

Figure 2.3: Schematic diagram: element arrangement of a linear phased array within a transducer. Elements (yellow circles) emit rays in phases.

The image formed closest to the transducer is the same width as the transducer. However, after this point the image fans out, thus a larger image is produced than with a linear sequential array transducer of the same size. The larger images produced from a smaller transducer make this array type ideal for imaging small or difficult to reach parts of the body. Furthermore as the elements within the transducer can be rotated, the image produced can be focused to a point of interest.

Curved Sequential Array

The transducer for a curved sequential array is, as the name suggests, curved (Figure 2.4). The elements are situated along the curve and therefore this array does not require the use of beam steering to produce a large image. Beams are emitted from the elements sequentially.

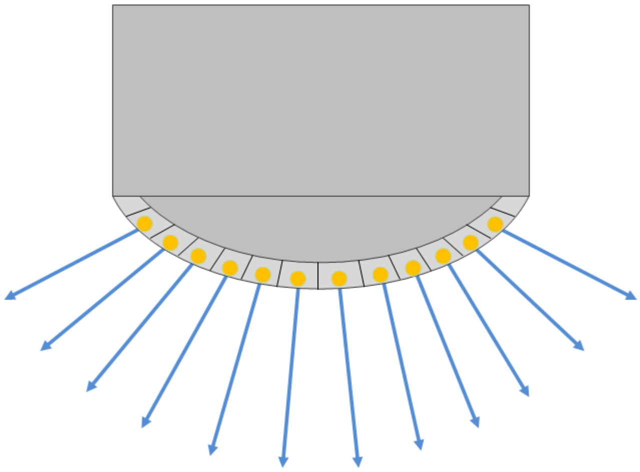

Figure 2.4: Schematic diagram: element arrangement of a curved sequential array within a transducer. Elements (yellow circles) emit US rays (blue arrows).

The curved array types are typically used to image large areas and use frequencies of around 2–5 MHz [14] in order to image areas deep within the body. The larger field of view is inappropriate for some imaging procedures such as images of the heart, hence the linear phased area is often used instead for cardiac ultrasounds [14]. As the rays fan out, the gaps between each individual ray increase further down the image. At the deepest points, the quality of the image is reduced.

2.4 Distortions in Medical Ultrasound Imaging

There are various factors that can account for the distortions seen in modern day images. These factors generally fall into two categories:

1. incorrect assumptions about the properties of the mediums involved,
2. incorrect assumptions about the behaviour of the ultrasound waves.

The first category mainly consists of assumptions with regards to the acoustic velocity of the mediums within the body, as well as the acoustic mediums within the transducers. Conversely, the second category concerns matters such as absorption, reflection strength, scattering effects, refraction and diffraction. If the properties of the media involved differ from the expected, the calculations involved to produce the images will incorporate incorrect information. This, along with the physical behaviour of the rays, can account for the distortions seen in ultrasound images known as artifacts.

When considering the structure of the image of a foetal head, the difference in the acoustic velocities involved are the most important to acknowledge. That is, the misrepresentation of distances due to incorporating the wrong acoustic velocities and ignoring the occurrence of refraction.

2.4.1 Physical Origins of Distortion

Refraction

The acoustic velocity of a medium depends upon the medium's density. When a ray hits a boundary between media of dissimilar densities, the fraction of the ray that transmits into the second medium is refracted. The angle of refraction, θ_2, is related to the angle of incidence, θ_1, and the acoustic velocities of the two mediums via Snell's Law,

$$\frac{\sin(\theta_1)}{\sin(\theta_2)} = \frac{c_1}{c_2}\,. \tag{2.2}$$

where c_1 and c_2 are the acoustic velocities of the two mediums. When $c_1 = c_2$, $\theta_1 = \theta_2$ and the ray is not refracted.

Figure 2.5 shows three cases of refraction. Figure 2.5(a) displays a refraction with an angle of incidence such that $0 \leq \theta_2 < \pi/2$. If $c_1 > c_2$ the ray will be refracted towards the normal at the point of impact. Conversely, if $c_1 < c_2$ the ray will be bent away from the normal. The types of refraction shown in Figure 2.5(b) and (c) are extreme cases of (a), when $c_1 < c_2$. When $\theta_2 = \pi/2$ (Figure 2.5(b)) the ray travels along the boundary between the two mediums. This 'critical' angle,

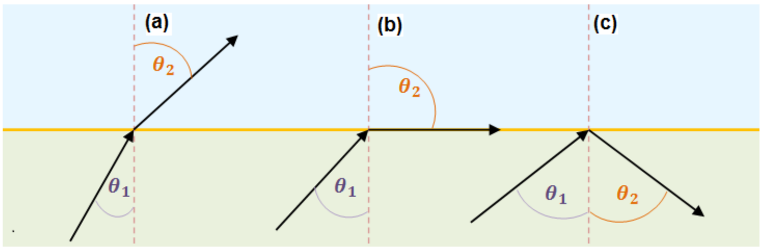

Figure 2.5: Three cases of refraction for a ray incident to a boundary between two mediums with acoustic velocities c_1 and c_2: (a) $0 \leq \theta_2 < \pi/2$, (b) $c_1 < c_2$, $\theta_1 = \theta_{crit}, \theta_2 = \pi/2$ (c) $c_1 < c_2$, $\theta_1 > \theta_{crit}$ (total internal reflection).

θ_{crit} therefore can be defined as,

$$\theta_{crit} = \arcsin\left(\frac{c_1}{c_2}\right) . \tag{2.3}$$

Angles of incidence greater than the critical angle ($\theta_1 > \theta_{crit}$) result in total internal reflection. In this case (Figure 2.5(c)) the ray does not transmit through to the second boundary.

Mismatch in Acoustic Impedance

At a boundary between mediums, providing that the mediums are of dissimilar densities, reflection occurs. The difference in the acoustic impedances of the mediums correspond to the strength of the echo produced. Acoustic impedance (Z) is defined as,

$$Z = \rho c ,$$

where ρ is the density and c is the acoustic velocity of the medium.

Consider two mediums, with acoustic impedances of Z_1 and Z_2. The fraction of the initial wave that is reflected (R) is,

$$R = \left(\frac{Z_2 - Z_1}{Z_2 + Z_1}\right)^2 .$$

Figure 2.6(a) shows a ray which does not reflect at the boundary. In fact, all of the ray transmits through to the second medium. This occurs when $Z_1 = Z_2$ (i.e. $R = 0$). If $Z_1 \approx Z_2$, as shown in Figure 2.6(b), only a small fraction of the ray is reflected and the rest transmits through. Complete reflection, Figure 2.6(c), occurs when $R = 1$, i.e the difference between Z_1 and Z_2 is very large.

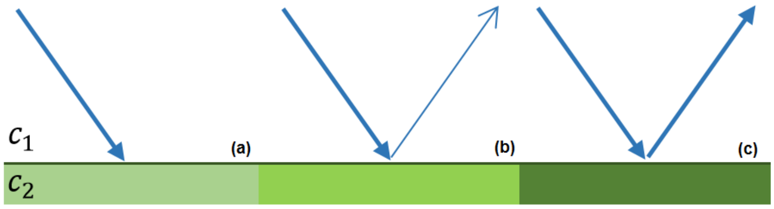

Figure 2.6: Strength of echoes for a ray incident on a boundary between media with acoustic impedances Z_1 and Z_2: (a) $Z_1 = Z_2$, no echo produced, (b) $Z_1 \approx Z_2$, weak echo produced, (c) difference between Z_1 and Z_2 great, strong echo produced.

Scattering

When a ray hits a smooth surface, a fraction of the ray is reflected and the rest transmitted through. This is not the case when a ray hits a rough surface. The ray instead is scattered in a non-uniform manner in all directions. The effect of scattering contributes to attenuation; the loss of energy of an ultrasound beam. Although blood cells and other media in the body are generally weak scatterers, bubbles within liquids - such as blood - are strong scatterers [11]. Indeed, this is the principle behind the used of 'micro-bubbles' to enhance contrast in US images.

Diffraction

Diffraction occurs when a wave encounters a slit as seen in Figure 2.7. The images produced by an ultrasound scanner work under the assumption that the beam travels like a series of light waves. When light is shone at an object with a slit, the light travels through the slit in straight lines. Waves, however, form a ripple with the centre of the slit as the centre of the ripple. Diffraction also occurs when a wave is emitted from a source, such as a transducer.

Figure 2.7: Wave travelling from left to right (blue), as the wave passes through a slit in a boundary (orange) diffraction occurs.

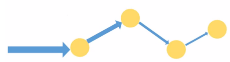

Figure 2.8: US ray travelling from left to right (blue), when the ray encounters an object, such as a molecule (yellow), some of its energy is absorbed by the object.

Absorption

As an ultrasound ray travels through the body, the tissues it passes through absorb some of its energy. It is tissue absorption of the sound energy that contributes to most of the attenuation of an ultrasound wave. Attenuation, the weakening of the sound energy as it passes through tissues (as shown in Figure 2.8), is also caused by the scattering, refraction, diffraction and reflection of the ultrasound beam. Ultrasound rays that are attenuated to a great extent will not be able to return to the transducer and be detected.

2.4.2 Artifacts

The term artifacts is used to define any section of an image that does not accurately characterise the anatomic structures present and the underlying reasons behind the appearance of artifacts are worth noting. There are many different artifacts associated with various false assumptions and errors. Below are just a few [6], with the last type of artifact (caused by velocity errors) the most relevant to consider in order to quantify the distortions seen in cross-sectional images of a foetal head.

Artifacts associated with multiple echoes

Ultrasound imaging works on the principle that an echo returns to the transducer after one single reflection and the time taken for the return of the echo is directly related to the depth of the boundary it encountered. Interesting cases of where this assumption is broken are reverberation, comet tail, ring-down and mirror image artifacts.

Reverberation artifacts

Consider two highly reflective parallel surfaces. A portion of the initial ray travels through the first surface and hits the second surface. The corresponding echo reaches the transducer and the image of the boundary appears in the correct location. However, some of the echo encounters the first boundary again and is reflected away from the transducer. This is represented in Figure 2.9(a).

Sequential echoes that reach the transducer have taken longer to return and hence the image they produce of the second boundary appears at a greater depth. Therefore the two parallel surfaces appear in images as a series of equidistantly-spaced boundaries. A typical reverberation artifact is shown in Figure 2.9(b).

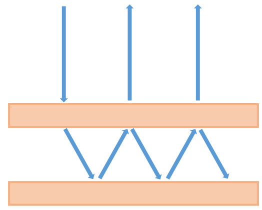

(a)Schematic diagram of the formation of a reverberation artifact.

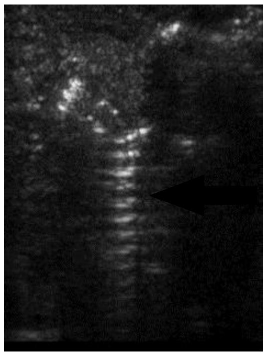

(b)Reverberation artifact [6]

Figure 2.9: (a)Ultrasound ray (blue) reflected between two parallel surfaces (orange). (b) Ultrasound image of a typical reverberation artifact.

Comet-tail artifacts

The comet-tail artifact is a type of reverberation artifact and occurs when two highly reflective surfaces are closely spaced to each other and cause the ultrasound ray to bounce between them.

The distances between the multiple false images of the second boundary may be indistinguishable and together form an object. Since the later echoes have a weaker amplitude due to attenuation, they portray the second boundary with a decreased width, therefore the object formed is tapered and triangular in appearance. An US image showing many comet-tail artifacts is shown in Figure 2.10.

Figure 2.10: US of a tumor in a thyroid with many comet-tail artifacts [16].

Ring-down artifacts

The ring-down artifact is often similar in appearance to the comet-tail artifact, however there are stark differences in the theory behind its creation.

The theory states that this particular artifact occurs when fluid is trapped between a tetrahedron of air bubbles (Figure 2.11(a)). The ultrasound energy transmitted resonates in the fluid and causes vibrations which create a continuous sound wave. This sound wave returns continuously, until eventual decay, to the transducer and the images formed from its detection appears as a line, as seen in Figure 2.11(b).

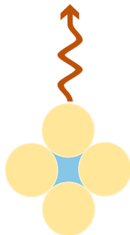

(a)Schematic diagram of ring-tail artifact causing molecule.

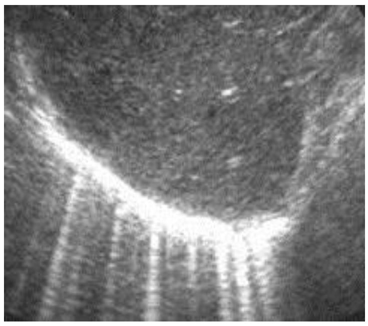

(b)Ring-down artifact [17].

Figure 2.11: (a) Oxygen molecules (yellow) trap fluid (blue) which vibrates when hit by an US ray and a signal (orange) is produced. (b) US image example of a ring-down artifact.

Mirror image artifacts

Mirror image artifacts occur when a particularly reflective surface is present, close to an object. An example which produces a mirror image artifact is of an object closer to the transducer than the reflective surface. This example is shown in Figure 2.12(a).

A portion of the rays that travel to the furthest boundary of the object are transmitted through the object to the reflective surface. Any rays that are reflected by this surface encounter the object again. Echoes that return from the second encounter with the object do so at a later point in time. These echoes cause a secondary image of the object to be produced at a greater depth.

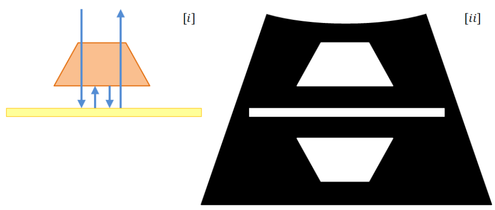

(a)Schematic diagram of a situation which causes a mirror image artifact and the artifact.

(b)Mirror image artifact [17].

Figure 2.12: (a) [i] Rays bounce in between an object (orange) and a reflective surface (yellow). [ii] Schematic diagram of the artifact produced by left. (b) US image of a mirror image artifact of the diaphragm and an object. Diaphragm acts as a strong reflective surface, real object on the right of the diaphragm.

Artifacts associated with attenuation errors

As an ultrasound ray travels through the body it is attenuated due to phenomena such as absorption and scatter. An echo which travels a greater distance is attenuated more than an echo of equivalent energy that travels a shorter route. To account for this, ultrasound processing incorporates compensation amplification of echoes. That is, echoes that return at later time points are amplified to make the image appear more uniform.

The compensation amplification process can have an adverse effect if a medium encountered in the deep field is weakly attenuating. The later echoes are not attenuated to the extent that would be expected for the large distance they have travelled and their amplitudes are not reduced to the degree anticipated. Therefore the amplification process returns a bright patch, called enhancement, on the image in the deep field (shown in Figure 2.13(a)).

Even with the compensation process in place, the strongest attenuating mediums reduce the amplitudes of the echoes to an extent which can not be detected by the transducer. Such an occurrence appears on the image as a dark band or a shadow (shown in Figure 2.13(b)). Attenuation is also reliant on the frequency of the ultrasound emitted from the transducer. Ultrasound waves with a greater frequency are subjected to a greater degree of attenuation. If the attenuation of a medium is great, the reduction of the shadow may be possible through choice of an appropriate frequency transducer.

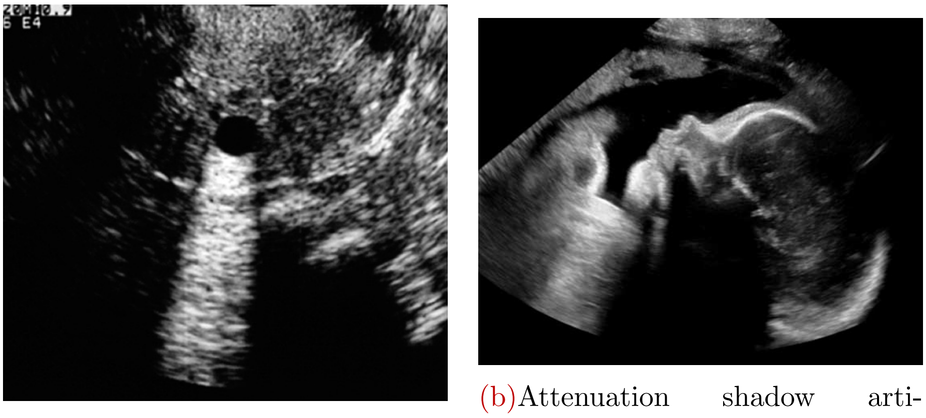

(a)Attenuation enhancement artifact. [18]

(b)Attenuation shadow artifact [18].

Figure 2.13: Attenuation artifacts: (a)US image of pelvic cyst containing low-attenuating fluid, with enhancement beyond. (b) US image of a foetal profile. The facial bones are strongly attenuating, causing shadow beyond.

Artifacts associated with velocity errors

Speed displacement and refraction artifacts are the two main artifacts associated with velocity errors. Speed displacement artifacts occur when all materials encountered by the ultrasound rays are assumed to have equal acoustic velocities. Therefore the images produced can appear closer or further away from the transducer than they are in reality. This speed displacement artifact is particularly evident when the ultrasound rays have travelled through a layer of fat, since the acoustic velocity of fat, approximately 1450 ms^{-1}, is significantly dissimilar to the assumed speed of 1540 ms^{-1}. Furthermore, ignoring the occurrence of refraction at boundaries between mediums of different densities produces refraction artifacts. This results in distortion in the size of an object and even discontinuities in the object's boundaries (Figure 2.15). The combination of these two artifacts are the most important to consider when quantifying the distortions that occur in a foetal head.

The assumed, calibrated (c_{cal}), speed at which ultrasound travels through the body is constant such that $c_{cal} = 1540$ ms^{-1}. In reality the real acoustic velocity (c_r) of various tissues and fluids differs from c_{cal}. Figure 2.14 is a plot of the acoustic velocities for a range of mediums within the body. It is evident from the graph that the c_r values can differ significantly from that of the calibrated speed. Note the c_r value for bone is excluded from Figure 2.14 and is approximately 4080 ms^{-1}. If $c_r < c_{cal}$, the distances between boundaries on the image will be greater than reality. Conversely if $c_r > c_{cal}$, the distances between boundaries on the image will be shorter than reality.

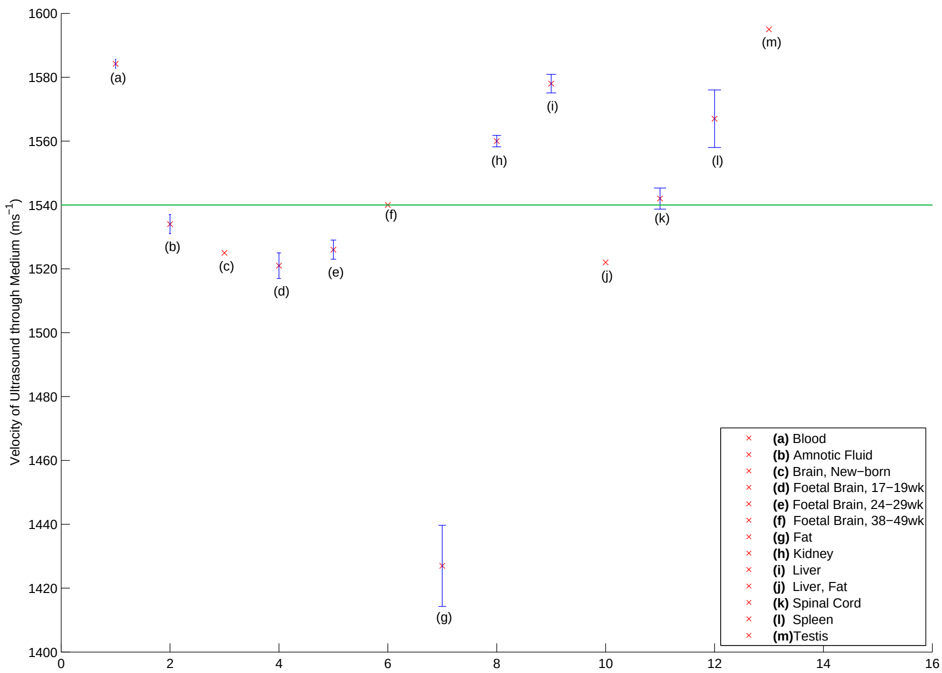

Figure 2.14: The acoustic velocity of different media within the body with values taken from [10]. The range of acoustic velocities for a particular medium are displayed in blue. The assumed velocity for the body, c_{cal}, is shown in green.

Figure 2.15: US of a cross-section of a foetal head, discontinuities in the skull arise due to velocity errors [18]

2.5 Physical Properties of a Foetus' Head

Obstetric ultrasonography is a standard part of prenatal care, used to visualise the embryo or foetus in the mother's womb. Different measurements are taken in order to estimate the gestational age of a foetus. One of the most accurate is the crown-rump length (CRL), which is measured at 7–13 weeks into the pregnancy. After 13 weeks the biparital diameter (BPD) can be calculated. The BPD is the width across the crown of the foetus' head (shown in Figure 2.16) and at 13 weeks should measure around 24mm and grow to around 95mm at term.

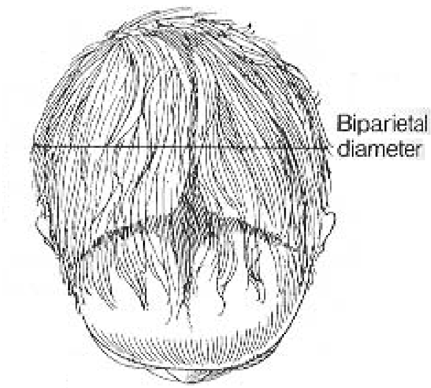

(a)Position of the BPD [19].

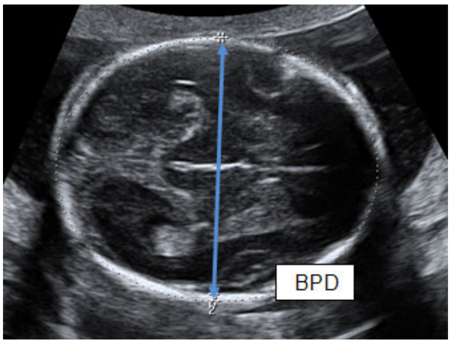

(b)Ultrasound image of BPD measurement [20].

Figure 2.16: (a) Drawing of the top of a foetus' head the BPD measurement is label. (b) US image of the cross- section of a foetus' head. The BPD is shown as a blue arrow across the head.

The gestational age of the foetus can also be calculated from the BPD. If the estimate of age disagrees with the one previously made from the CRL measurement, this can indicate that the foetus is not growing properly.

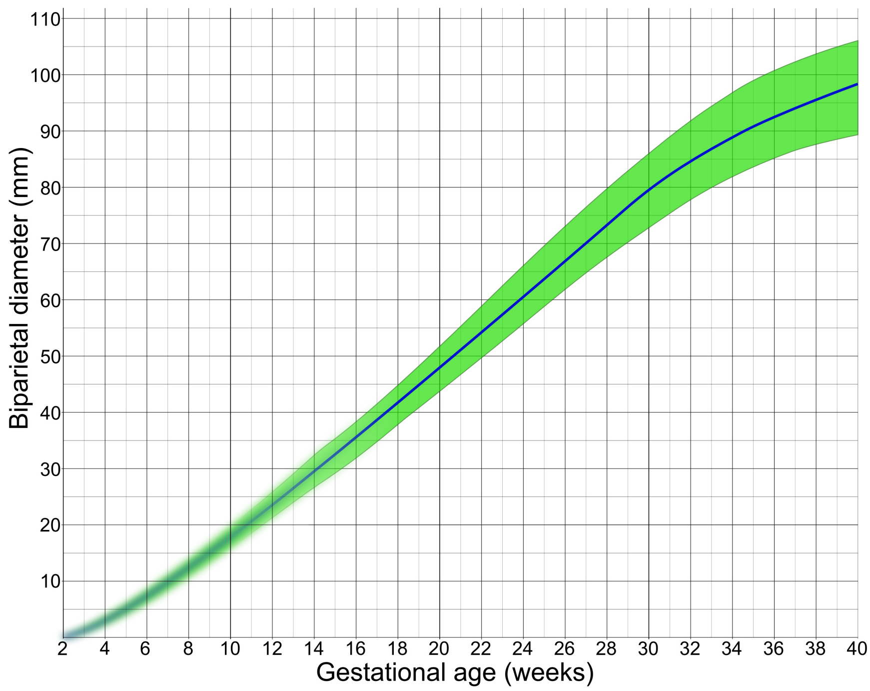

Figure 2.17: Biparietal diameter of a foetus by gestational age, with blue line representing the mean and the green area representing the 90% prediction interval. In addition to data taken from this study, the diagram is extrapolated from 0 to 14 weeks of gestational age by the rationale that it is 0 by fertilization at 2 weeks of gestational age [23].

During pregnancy the foetus grows inside an amniotic sack. The acoustic velocity of amniotic fluid is approximately 1540 ms^{-1} and therefore is not too dissimilar from the calibrated speed. The image of the 2D slice of the foetus' head, if subjected to little distortion, should take the form of an ellipse. The two important acoustic velocities to consider for the foetus' head are that of the foetus' skull and the foetus' brain.

The foetus' brain at 17–19 weeks has an acoustic velocity of approximately 1520 ms^{-1}, which corresponds to a BPD of around 42mm for a healthy foetus (Figure 2.17). The acoustic velocity for bone is around 4080 ms^{-1} in an adult. However, as a foetus' skull is soft and undeveloped the acoustic velocity should be much smaller.

The foetal skull is made up of different parts of bone which are not properly

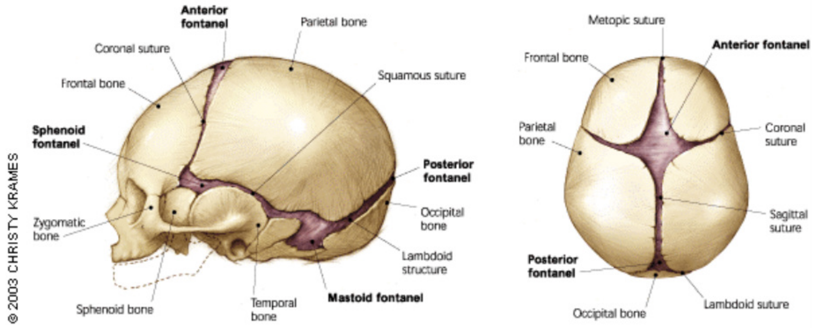

Figure 2.18: Structure of the skull

fused together and the gaps (fontanelles) between the cranial bones are covered by fibrous membrane - which is thin in comparision to the rest of the skull. The cross section of the skull of concern includes the frontal, parietal and occipital bones (the structure of the skull is shown in Figure 2.18).The thickness of the foetal skull varies throughout the pregnancy, but is known to be approximately 2mm at some point [21]. As the foetus' skull is very thin at around 2mm and accounts for less than 5% of the total width, a model without a skull is first considered in Chapter 4. Including the skull in the model requires the consideration of three acoustic velocities, c_1, c_2 and c_3, which are the acoustic velocities of the amniotic fluid, the skull and the brain respectively.

The acoustic velocity of the tibia bone in a foetus at a gestational age of 26 weeks is approximately 2800 ms^{-1} [22] . The acoustic velocity value of the foetal skull at 18 weeks is likely to be less than this and should also be larger than the value of the brain at 18 weeks ($\approx$ 1520 ms^{-1}). The models in Chapter 5 is originally constructed using an acoustic velocity of 2200 ms^{-1} and a thickness of 2mm for the skull. The values of the acoustic velocity of the brain and the amniotic fluid remain the same as in Chapter 4 (1520 ms^{-1} and 1540 ms^{-1} respectively). Furthermore the models are constructed with the assumption that the skull and brain are acoustically homogeneous. The only media considered in Chapter 5 are the foetal skull, brain and amniotic fluid. All other media, such as the skin, are ignored from the models.

3 Distortion of a Dot

In Chapter 5 this report aims to explore the distortions that occur in a cross-sectional image of a foetal head. As boundaries between media, such as the skull and the brain, can be thought of as a series of dots, the distortions in image of a single dot is first explored in this Chapter. Albert Goldstein considered this problem in 1999 [1] for four different array types. The images produced under the linear sequential array are mathematically the most simple to calculate and it is for this reason that the linear sequential array, along with the curved sequential array - which is medically the most commonly used transducer type [14], are the focus for this report.

Consider a single dot P_r, with negligible area, within a medium. When considering the single dot's image, the medium within the dot and the shape of the dot's image need not be considered. The main cause of the shift in position of the dot's image is due to the disagreement of the real acoustic velocity of the medium, c_r, with the calibrated acoustic velocity, c_{cal}. In this simple problem one can imagine that a single ray from the transducer would be responsible for the position of the image.

3.1 Linear Sequential Array

Consider the front, ray emitting, side of the transducer to be placed along the x-axis and a point $P_r = (x_r, y_r)$ in the positive (x, y)-plane, as shown in Figure 3.1. The position of the image of P_r ($P_i = (x_i, y_i)$) is calculated as follows.

First, the echo time T of flight is required. In practice, T would be the time between emission and detection. This would be recorded by the device and need not be calculated. However since in this model the real-space position of P_r is known, T can be calculated as,

$$T = \frac{2D_r}{c_r}\,,$$

where D_r is the real-space distance of P_r from the transducer and $D_r > 0$, since T is time taken for the ultrasound ray to travel from the transducer to P_r and return. The scanner is calibrated to correspond to tissues' acoustic velocity c_{cal} and so the image distance of P_i (D_i) from the transducer is,

$$D_i = \frac{1}{2} c_{cal} T\,. \tag{3.1}$$

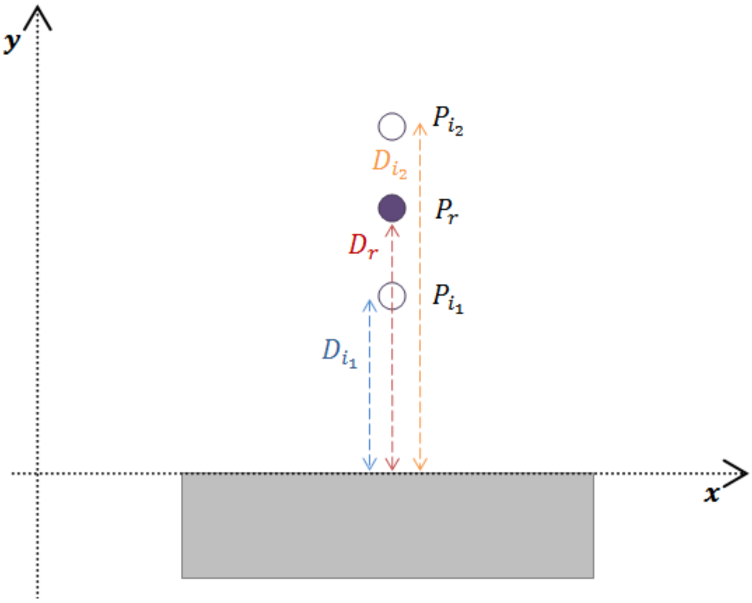

Figure 3.1: Linear sequential array set-up: the transducer shown in grey, P_r (filled purple dot) is the position of the dot in real-space. The position of the image is P_{i_1} for $c_r < c_{cal}$ and P_{i_2} for $c_r > c_{cal}$ (unfilled dots).D_{i_1}, D_{i_2} and D_r represent the distances from the transducer for the corresponding P values.

The change in the (x, y)-coordinates from P_r to P_i, Δx and Δy, are

$$\Delta x = 0$$

and

$$\Delta y = D_i - D_r\,.$$

Since $y_r = D_r$, the coordinates of P_i are

$$x_i = x_r\,, \tag{3.2}$$

and

$$y_i = D_i\,. \tag{3.3}$$

For linear arrays the misrepresentation is purely one-dimensional (as shown in Figure 3.2) and P_i is simply a translation of P_r in the vertical direction. It is for this reason that images produced by the linear array are often referred to as the most accurate of the two considered. Figure 3.2(a) shows the image of a series of dots which form a boundary. The image of the line for $c_r > c_{cal}$ is shown closer to the transducer than the real line. Conversely, images which have been calculated for $c_r < c_{cal}$, are shown further away from the transducer. The images of the line, for all values of c_r, retain a gradient of zero, with no discontinuities or 'wiggles'.

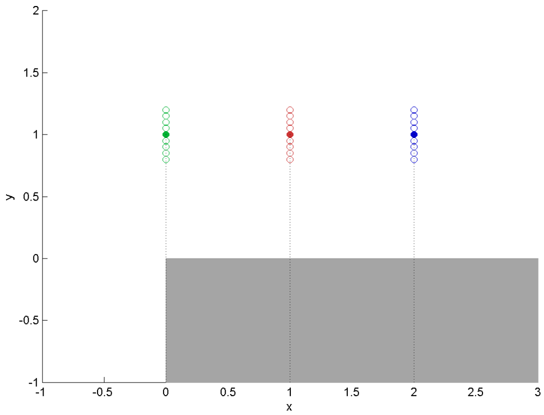

(a)Images of three dots for different c_r values

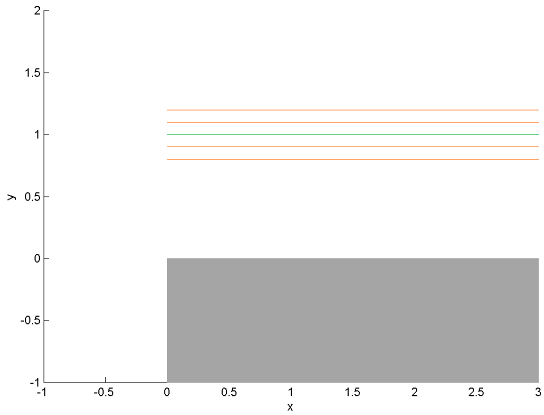

(b)Images of a line for different c_r values

Figure 3.2: Linear Sequential Array: transducer shown in grey (a)three dots (filled) and images produced (unfilled) for acoustic velocity ratios $c_r/c_{cal} = 0.80, 0.85, 0.90, 0.95, 1.05, 1.10, 1.15, 1.20$ shown from top to bottom. (b) Line (green) and images produced (orange) for acoustic velocity ratios $c_r/c_{cal} = 0.80, 0.90, 1.10, 1.20$, shown from top to bottom.

3.2 Curved Sequential Array

The image P_i produced under the convex array is not merely a 1D translation of P_r. Here

$$D_r = \sqrt{x_r^2 + y_r^2}\,,$$

as the ray which encounters P_r is not perpendicular to the x-axis as with the case of the linear array. To simplify the calculation, the centre of the transducer is taken to be along the line $x = 0$ - with the point $(0, 0)$ on the outside of the transducer, as shown in Figure 3.3.

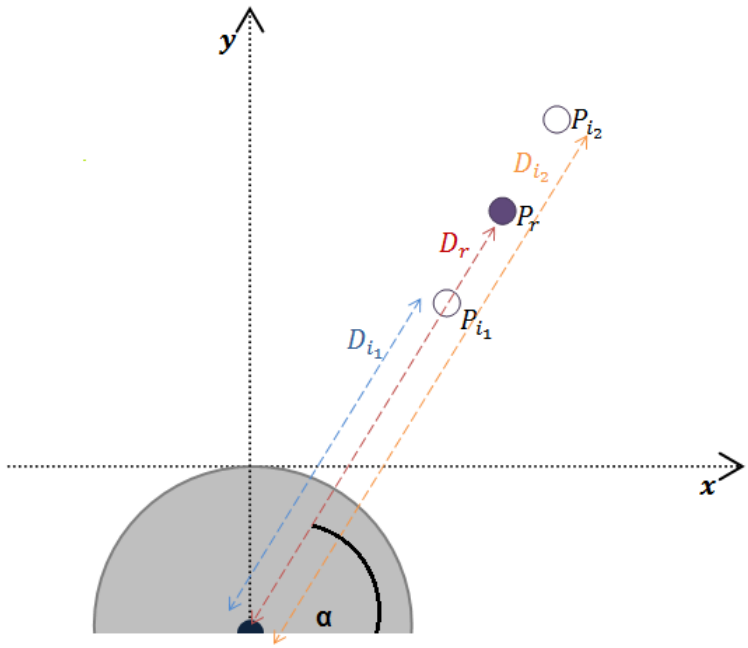

Figure 3.3: Curved sequential array set-up: the transducer shown in grey, P_r (filled purple dot) is the position of the dot in real-space. The position of the image is P_{i_1} for $c_r < c_{cal}$ and P_{i_2} for $c_r > c_{cal}$ (unfilled dots). D_{i_1}, D_{i_2} and D_r represent the distances from the transducer for the corresponding P values. The angle α is the angle between the x-axis and the ray that is incident to P_r

The distance from the transducer and the image point, D_i, is calculated in the same way as equation (3.1) and therefore for the curved sequential array,

$$\Delta x = D_i \cos(\theta) - x_r$$

and

$$\Delta y = D_i \sin(\theta) - y_r \,,$$

where θ is the angle between the ultrasound ray and the x-axis.

The coordinates of P_i are,

$$x_i = D_i \cos(\theta)$$

and

$$y_i = D_i \sin(\theta) \,.$$

Taking $\theta = \pi/2$, which is the value of θ for the linear array, returns the x_i and y_i values seen in equations (3.2) and (3.3).

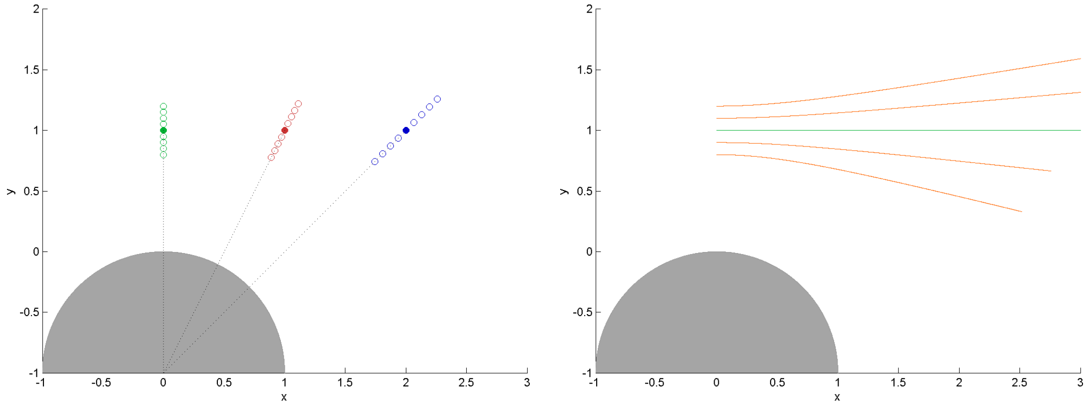

(a)Images of three dots for different c_r values.

(b)Images of a line for different c_r values.

Figure 3.4: Curved Sequential Array: transducer shown in grey. (a)Three dots (filled) and images produced (unfilled) for acoustic velocity ratios $c_r/c_{cal} = 0.80, 0.85, 0.90, 0.95, 1.05, 1.10, 1.15, 1.20$, shown from top to bottom. (b) Line (green) and images produced (orange) for acoustic velocity ratios $c_r/c_{cal} = 0.80, 0.90, 1.10, 1.20$, shown from top to bottom.

Figure 3.4(a) displays how the value of α (the angle between the x-axis and the ray) affects the position of the image. At $\alpha = \frac{\pi}{2}$ the position of the image does not vary in the x direction and the image is the same as seen by the linear array in Figure 3.2(a). As $\alpha \to 0$ the values of Δx and Δy increase. Figure 3.4(b) portrays how a line is distorted in its image. Unlike the images produced under the linear sequential array in Figure 3.2(b), the images of the line are curved. Images of the line produced with a greater disagreement of c_r in comparison to c_{cal} curve to a greater degree than the images produced with $c_r \approx c_{cal}$.

Figure 3.2 and Figure 3.4 show that an image of a dot is subject to some degree of distortion, relative to the difference between the calibrated velocity, c_{cal}, and the real acoustic velocity, c_r. A larger disagreement in the two acoustic velocity values results in a greater distortion. In addition, the figures suggest that images produced with a curved sequential array are more distorted. Chapter 4 builds upon the ideas presented here, to evaluate the distortions of images of circular objects (i.e. circles and ellipses).

4 Distortion of Circular Objects

4.1 Modelling Images of Circular Objects with a Linear Sequential Array

In Chapter 3, the distortions of a dot are discussed. The boundaries between media can be treated as a series of these dots. As a crude approximation, the foetus' head can be modelled as an elliptic object within a medium of a lower density. In Chapter 5 a model which includes the skull is considered, however this Chapter is concerned with the distortion of an ellipse alone.

In order to better understand the effects of varying the acoustic speeds of objects and their surrounding mediums, a simple ray model for the distortion of the image for a circle - as opposed to an ellipse which represents a foetus' head more accurately - is the focus of this Chapter. For the model of the artifacts caused by the linear sequential array, the assumption is made that the transducer is at least the size of the circle or ellipse being imaged.

The boundary of the circle is constructed as a series of individual points. A single ray within the ultrasound beam is responsible for the position of the image for an individual point. It is assumed the linear sequential array emits individual horizontal parallel beams.

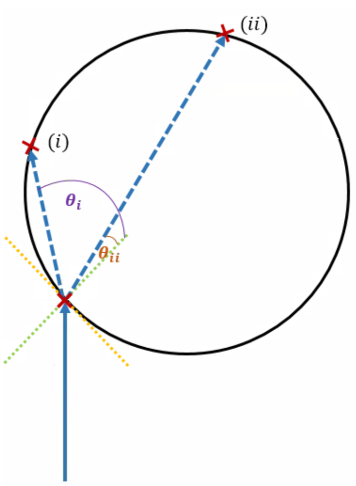

Figure 4.1: Schematic diagram: a single ray (blue solid) produced by a linear sequential array type transducer incident to the lower side of a circle, at the point the tangent line is shown in yellow (dashed) and the normal line in green (dashed). (i) The path (blue dashed) the ray could take if $c_1 < c_2$ with the angle of refraction θ_i .(ii) The path (blue dashed) the ray could take if $c_1 > c_2$ with the angle of refraction θ_{ii}.

The transducer is placed below the circle such that the rays first encounter the lower side of the circle, before reaching the upper side as shown in Figure 4.1. When a ray hits a point P_L on the lower boundary of the circle, it is refracted, as dictated by Snell's Law. If $c_1 < c_2$, where c_1 is the acoustic velocity of the surrounding medium and c_2 is the acoustic velocity of the medium within the circle, the ray will be refracted away from the normal at P_L (shown by (i) on Figure 4.1). Conversely, if $c_1 > c_2$, the ray is refracted towards the normal at point P_L (shown by (ii) on Figure 4.1). Rays at point P_L are not refracted if $c_1 = c_2$.

Rays travel through the circle until reaching a point on the upper boundary of the circle, P_U. At both points, P_L and P_U, part of the ray is reflected back towards the transducer. It is assumed that the individual rays travel back along the path they originally took. At the point P_U, part of the ray is refracted through and this is ignored as the ray will never return to the transducer.

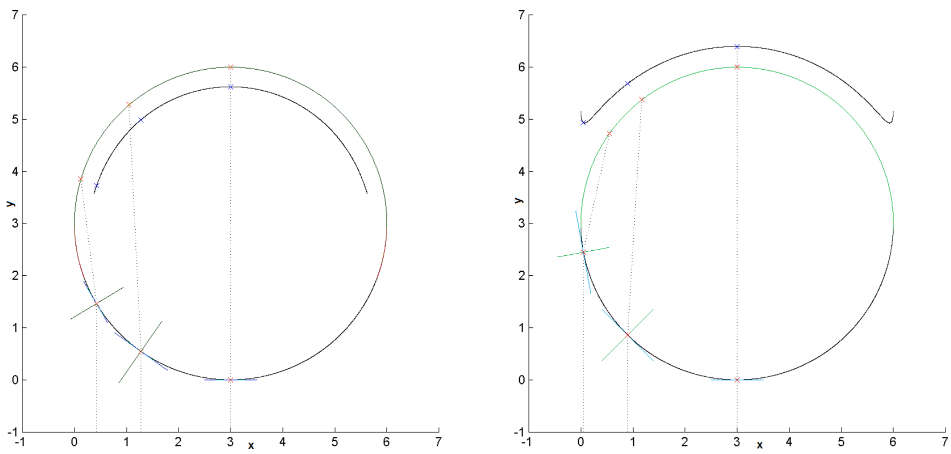

(a)$c_1 < c_2$. (b)$c_1 > c_2$.

Figure 4.2: Image artifact model for linear sequential array: rays that are totally internally reflected and do not reach the upper boundary are coloured in red on the circle. Three arbitrary rays are shown in black (dashed), points of intersection of rays and boundaries shown in red ('x') and corresponding image points in blue ('x') (a)$c_1 = 0.95c_2$ ($c_1 < c_2$) (b) $c_1 = 1.05c_2$ ($c_1 > c_2$).

Figure 4.2 shows the outcome of modelling the distortion of an image of a circle, using the ray model, for two cases. The axes are arbitrary and unit-less, but for the sake of ease, the vertical axis is referred to as the y-axis and the horizontal, the x. In Figure 4.2(a) $c_1 = 0.95c_2$ ($c_1 < c_2$) and in Figure 4.2(b), $c_1 = 1.05c_2$ ($c_1 > c_2$). As predicted, the lower side of the circle is accurately represented by its image in graphs. The portion of the rays that are subjected to total internal reflection are shown in red. The case represented by Figure 4.2(a) is subjected to occurrences of total internal reflection.

The upper side of the circle in case Figure 4.2(a) is portrayed in the image as closer to the transducer than in reality. Due to the total internal reflection that occurs, the image is shorter than the reality. Probably the most intriguing aspect of distortion occurs in Figure 4.2(b), as $x \to 0$ and $x \to 6$, in the upper part of the circle. The image for the extreme cases of x 'flick' up. The actual distance between the point the ray hits on the lower ellipse and the extreme cases of x on the upper ellipse is very slight. However the degree of refraction that occurs at the lower circle means the ray gets bent towards the centre of the circle and travels further than it should have. The greater the discrepancy in the speeds, the larger the 'flicks'.

4.1.1 Distortion of an Ellipse with a Linear Array

In Chapter 5, the distortion which occurs in the image of a foetal head is explored. The ellipse required should represent the correct widths and ratios for a foetal head, as well as including the approximate values for the acoustic velocity of all the media involved. The BPD and the perpendicular measurement occipitofrontal diameter (OFD) are available, for a wide range of ages, via existing data.

Weeks	BPD (mm)	OFD (mm)	HC (mm)
17	39 (5.0)	50 (3.0)	141 (15)
18	42 (4.0)	54 (3.5)	151 (20)
19	45 (5.0	57 (3.5)	160 (20)

Table 1: Dimensions, biparietal diameter (BPD), occipitofrontal diameter (OD) and head circumference (HC) of a foetus for gestational ages 17–19 weeks.

The model used to construct the graphs seen in Figure 4.2 is adapted to correspond to the values for a foetus at 18 weeks. Table 1 shows the values of the BPD and the OFD for the gestational ages of 17–19 weeks. The model is constructed using the values corresponding to a gestational age of 18 weeks (BPD:42mm, OFD:54mm). The acoustic velocities are set to correspond to the approximate acoustic media of the amniotic fluid and foetal brain, $c_1 = 1540$ ms^{-1} and $c_2 = 1520$ ms^{-1} respectively.

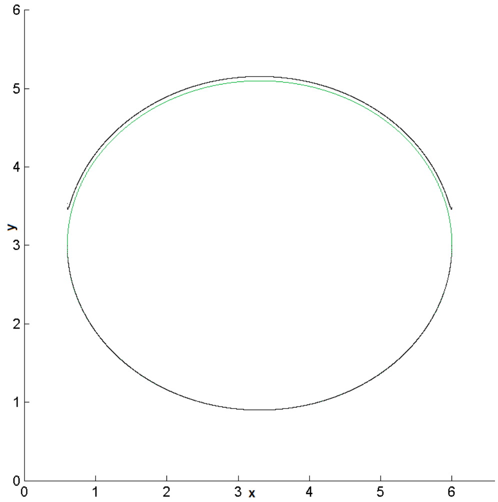

Figure 4.3: The image (black) of an ellipse for the linear sequential array. The acoustic velocities are $c_1 = 1540$ ms^{-1} (outside the ellipse) and $c_2 = 1520$ ms^{-1} (inside the ellipse).

Figure 4.3 shows the result of adapting the circular model to correspond to a foetus at 18 weeks. Here $c_1 \approx 1.01c_2$ ($c_1 > c_2$) and the distortion is more subtle than seen in Figure 4.2(a). This agrees with the discussion in Chapter 3, that the larger the difference in the speeds of the mediums, the greater the distortion of the image. Figure 2.15, a real cross-sectional US image of a foetus' head, shows similar gaps in the head as seen in Figure 4.3. However, due to the shape of the image, it is clear Figure 2.15 was not produced with a linear sequential array. The next section looks at a model for circular objects imaged by the curved sequential array, which is a likely candidate for the production of the image of the foetus' head in Figure 2.15.

4.2 Modelling Circular Objects with a Curved Sequential Array

Returning to a circle, a similar model to the one in Section 4.1.1 is developed for the curved sequential array. Unlike its linear counterpart, the rays emitted from the curved array will not reach all of the lower side of the circle. Figure 4.4 diplays the set-up for this model.

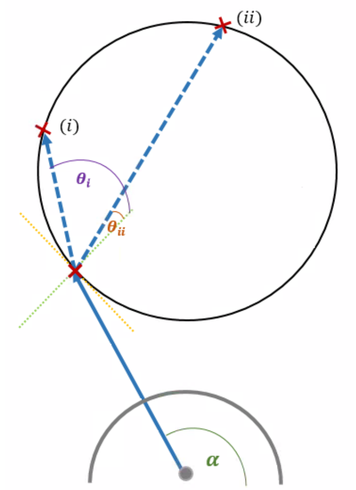

Figure 4.4: Schematic diagram: a single ray (blue solid) produced by a curved sequential array type transducer incident to the lower side of a circle, at the point the tangent line is shown in yellow (dashed) and the normal line in green (dashed), the angle α is the angle of the ray from the x-axis. (i) The path (blue dashed) the ray could take if $c_1 < c_2$ with the angle of refraction θ_i. (ii) The path (blue dashed) the ray could take if $c_1 > c_2$ with the angle of refraction θ_{ii}.

Figure 4.5(a) and Figure 4.5(b) have the same parameters as Figure 4.2(a) and Figure 4.2(b) respectively. Regarding the position of the upper boundary, the two sets of figures are similar. However the 'flicks' that were present in Figure 4.2(b) are not displayed on Figure 4.5(b). The graphs in Figure 4.5, unlike those in Figure 4.2, do not provide a full accurate representation of the lower side of the circle. The range of rays that would be refracted to a greater degree, like those near $x = 0$ and $x = 6$ which caused the 'flicks' in Figure 4.2(a), never actually hit the circle in Figure 4.5(b).

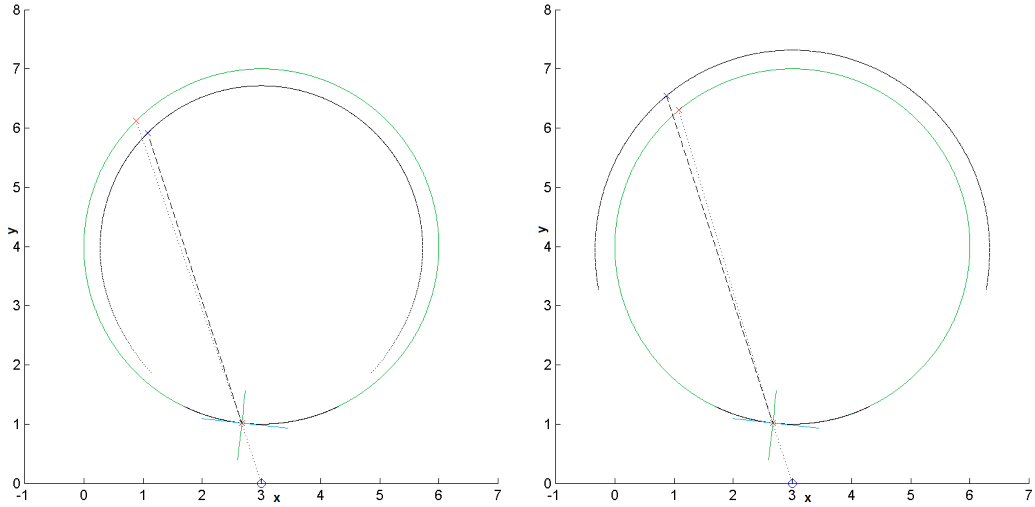

(a)$c_1 < c_2$ (b)$c_1 > c_2$

Figure 4.5: Image artifact model for curved sequential array: image (black). (a) The acoustic velocities of the mediums are $c_1 = 0.95c_2$ ($c_1 < c_2$)(b)The acoustic velocities of the mediums are $c_1 = 1.05c_2$ ($c_1 > c_2$).

4.2.1 Distortion of an Ellipse with a Curved Array

The model used in Section 4.2 can be adapted using the same dimensions given in Section 4.1.1. The result of using a curved sequential array for the ellipse with the parameters corresponding to a foetus at gestational age of 18 weeks is seen in Figure 4.6. The discontinuity occurs at a lower y value than seen in Figure 4.3. A larger fraction of the rays impact upon the lower side of the ellipse, than they do in the case of the circle in Figure 4.5, as the change in gradient over the lower ellipse is gradual in comparison to the circle. Since a larger fraction of the lower ellipse is impacted, a few of the rays that experience the greater degree of refraction that causes the 'flicks' are included. As $c_1 \approx c_2$, the flicks are hardly discernible. Again considering Figure 2.15, Figure 4.6 displays a similar discontinuity in the boundary of the head.

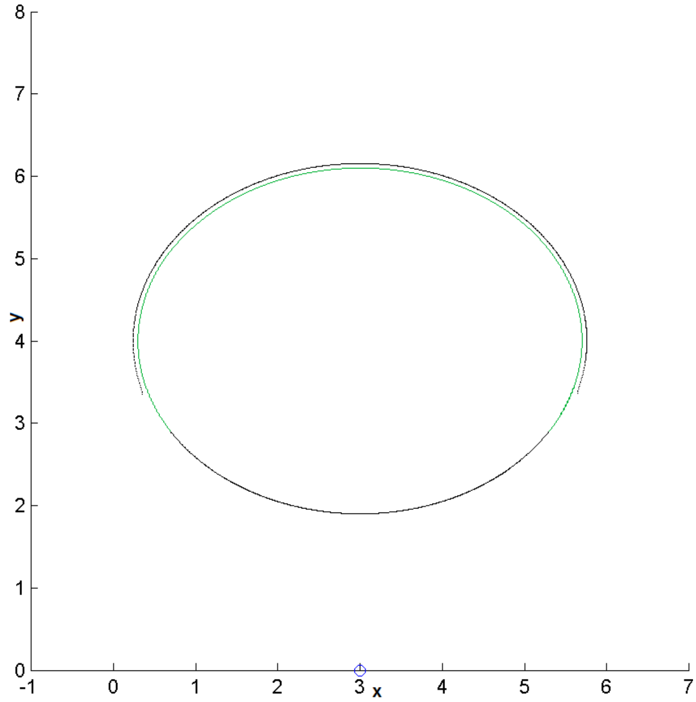

Figure 4.6: The image (black) of an ellipse for the linear sequential array. The acoustic velocities are $c_1 = 1540$ ms^{-1} (outside the ellipse) and $c_2 = 1520$ ms^{-1} (inside the ellipse).

This Chapter has explored the distortions of images for circular objects, for the linear and curved sequential arrays. Both arrays have produced more distortion of the upper boundary than the lower. The models with parameters corresponding to a cross-sectional image of a foetus' head at 18 weeks display similar behaviour to US images such as Figure 2.15, i.e. the images retain a general elliptic shape, but contain discontinuities. In Chapter 5, these models are adapted to include a layer of soft-undeveloped bone, namely the foetal skull. Including the skull in the model should provide a fuller picture of the distortions that arise.

5 Distortions of a Foetal Head

5.1 Modelling a Cross-Section of a Foetus' Head with a Linear Sequential Array

Inclusion of the skull in the model requires the consideration of three different speeds. It is assumed that c_2, the acoustic velocity of the skull, is always greater than the acoustic velocity of the amniotic fluid and the brain, c_1 and c_3 respectively. The cases where $c_2 < c_1$ and or $c_2 < c_3$ are ignored. The parameters of the foetal head model are shown in Table 2 and represented schematically in Figure 5.1.

Parameter	Numerical Value
a_1	2.7cm
b_1	2.1cm
a_2	2.5cm
b_2	1.9cm
w_0	4.0cm
z_0	4.0cm
c_1	1540 ms^{-1}
c_2	2200 ms^{-1}
c_3	1520 ms^{-1}

Table 2: Table of Parameters used for Figure 5.2 and Figure 5.3

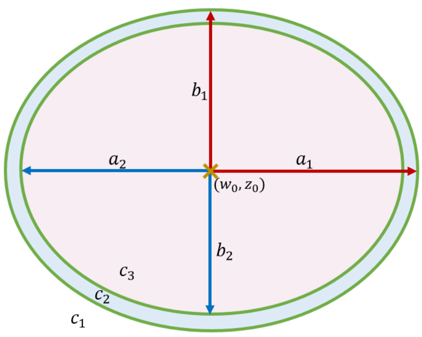

Figure 5.1: Schematic diagram of the parameters used in Figure 5.2.

The dimensions and acoustic velocities described in Section 2.5 and displayed in Table 2 are used in the model for the artifact produced by the linear array and is shown in Figure 5.2. The linear array model, when compared to the curved array model, should produce an image that is closer to the true object. However, linear transducer arrays are rarely used in obstetrics as the transducer head is long and flat and the mother's stomach is round [11]. Therefore a range of values for the properties of the skull are considered in Section 5.2 for the more commonly used curved sequential array only.

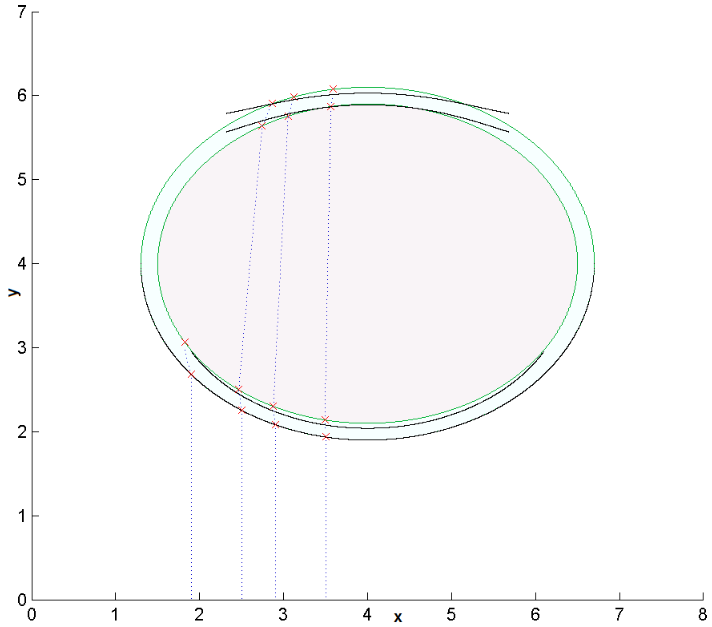

Figure 5.2: Cross-section of a foetal head, skull (light blue), foetal brain (pink). Image (black) produced by the linear sequential array, with parameters from Table 2. A selection of ray paths (blue dashed) are shown. The points of impact of a ray with a boundary between media are shown in red ('x').

Figure 5.2 shows the image of the cross-section of a foetus' head which has a width of 2mm and an acoustic velocity of 2200 ms^{-1} for the foetal skull. The top section of the image doesn't mimic its real-space counterpart as well as the image of the lower section. Observing US images such as Figure 2.15 suggest that the parameters for the properties of the skull are incorrect, if the model is working correctly. There a number of 'checks' that can be performed to support the theory that the model is working as expected. Two of which are:

1. check that if all the acoustic speeds are equal, $c_1 = c_2 = c_3$, no refraction occurs,

2. calculate the distances involved for the simplest point, i.e. the point with a tangent with zero gradient ($x = 4$ on Figure 5.2), where no refraction is involved and compare to the model.

5.2 Modelling a Cross-Section of a Foetus' Head with a Curved Sequential Array

The model for the artifacts produced with the curved sequential array follows a similar method to that of the linear sequential array but with the added complexity that the rays approach the lower boundary at an angle.

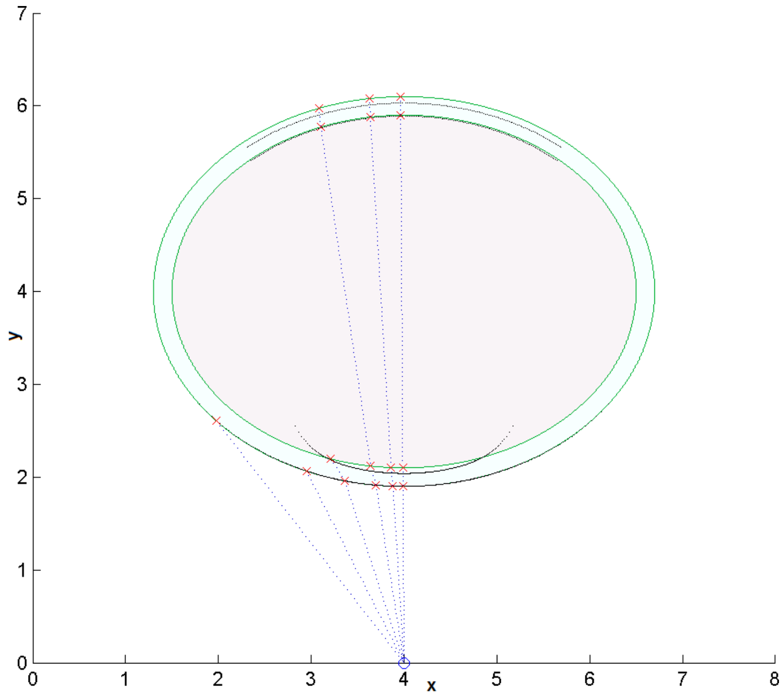

Figure 5.3: Cross-section of a foetal head, skull (light blue), foetal brain (pink), representative point of ray emission (blue unfilled dot). Image (black) produced by the curved sequential array, with parameters from Table 2. A selection of ray paths (blue dashed) are shown. The points of impact of a ray with a boundary between media are shown red ('x').

Figure 5.3 displays the distortion of a cross-section of a foetal head with the same parameters as Figure 5.2 for the curved sequential array transducer. This particular graph is not exceedingly convincing as a model for the distortions seen in real US images. The main discrepancy between Figure 5.3 and images like Figure 2.15, is the image of the inner lower skull. A similar phenomena to that which caused the 'flicks' in Figure 4.2(b) creates the steeper curve. Rays experience a greater degree of reflection at the extremal values of x and therefore travel further through the skull. The increase in the angle of refraction towards the edges of the ellipse effect the image more than the discrepancy between c_2 and c_{cal}, which is still used as the assumed speed to calculate the distances of the image points. The rays which produce the extreme image points of the lower inner skull are totally internally reflected, so do not continue to the next boundary. This accounts for the seemingly rational images at the furthest two boundaries.

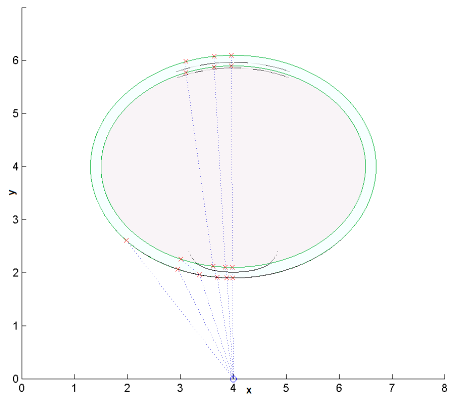

(a) a_2 =2.5cm, b_2 =1.9cm (2mm), c_2= 2800 ms^{-1}

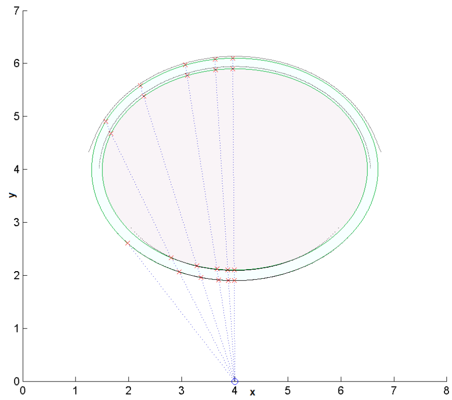

(b) a_2 =2.5cm, b_2 =1.9cm (2mm), c_2= 1600 ms^{-1}

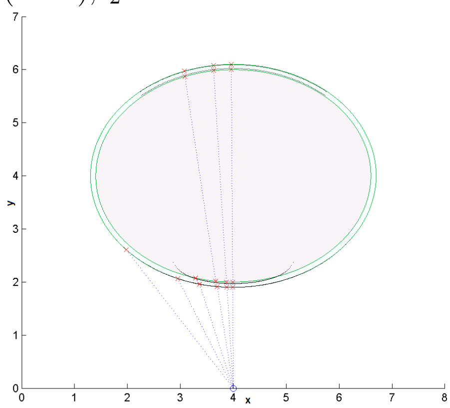

(c) a_2 =2.6cm, b_2 = 2.0cm (1mm), c_2= 2200 ms^{-1}

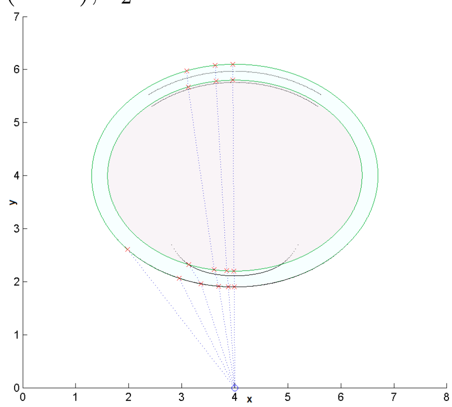

(d) a_2 = 2.4cm, b_2 = 1.8cm (3mm), c_2= 2200 ms^{-1}

Figure 5.4: Cross-section of a foetal head, skull (light blue), foetal brain (pink), representative point of ray emission (blue unfilled dot). Image (black) produced by the curved sequential array for a_1 = 2.7cm, b_1 = 2.1cm, c_1=1540 ms^{-1}, c_3=1520 ms^{-1} and varying parameters for a_2, b_2 (with corresponding width of the skull in brackets) and c_2. A selection of ray paths (blue dashed) are shown. The points of impact of a ray with a boundary between media are shown in red ('x').

Figure 5.4 contains four graphs which represent the images that may be produced for varying acoustic velocity values for the skull and the skull width. It was assumed in Section 2.5 that $1540 < c_2 < 2800$. Figure 5.4(a) and Figure 5.4(b) have different c_2 values to Figure 5.3, however in all other parameter values are the same. The effect of adjusting the c_2 values have a drastic effect on the top two boundary image lines. Figure 5.4(b) appears to relate closer to US images, such as Figure 2.15, out of the two.

The next two figures, Figure 5.4(c) and Figure 5.4(d), vary the skull width relative to Figure 5.3 which uses 2mm as an approximation for the skull width as discussed in Section 2.5. Varying the skull width only effects the distances between the boundaries, not the actual image shape.

From Figure 5.4 it could be argued that Figure 5.4(b) is the most appropriate figure out of the five considered. Since the width of the skull does not affect the shape of the image, just the width of the image of the skull, an estimate from the width would require closer evaluation of US images such as Figure 2.15. Assuming, for the sake of argument, that the width of the skull is smaller than the original estimate, a combination of Figure 5.4(b) and Figure 5.4(c) is shown in Figure 5.5.

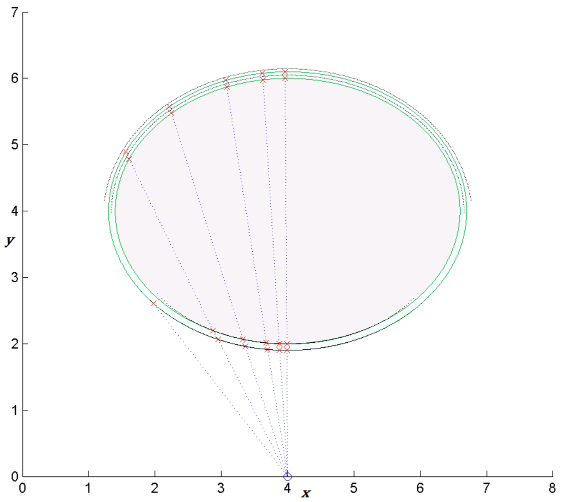

Figure 5.5: Cross-section of a foetal head, skull (light blue), foetal brain (pink), representative point of ray emission (blue unfilled dot). Image (black) produced by the curved sequential array for $a_1 = 2.7$cm, $b_1 = 2.1$cm, $a_2 = 2.6$cm, $b_2 = 2.0$cm (skull width 1mm), c_1=1540 ms^{-1}, c_2=1600 ms^{-1}, c_3=1520 ms^{-1}. A selection of ray paths (blue dashed) are shown. The points of impact of a ray with a boundary between media are shown (red 'x').

Further analysis is required to decide whether Figure 5.3 or Figure 5.5 is the most appropriate for modelling of a velocity artifact for the distortion of the cross-sectional image of a foetal head. A model that could accurately model the distortions, could be used to quantify the distortions and highlight whether techniques need to be employed to improve the accuracy of US imaging procedures.

6 Conclusions and Further Work

Ultrasound scans are a favoured imaging modality amongst diagnosticians. The images are often relied upon to provide accurate information about lengths and areas of structures within the body. It is important to quantify any distortions that occur in an US image to assess the need for new imaging techniques with greater precision.

This report discussed the technicalities of using ultrasound as an imaging device. Different distortions (artifacts) were described and the physical reasons for their appearance suggested. The important concept of refraction of rays between media of difference densities was introduced, along with Snell's Law which describes the angles which dictate refraction.

In Chapter 3 the distortion of the image of a dot was calculated for two common array types, following the methods set out by Goldstein in 1999. The results from this Chapter formed the basis for the modules produced in the proceeding Chapters.

Chapter 4 investigated the distortions of circular objects, in particular circles with $c_1 = 0.95c_2$ and $c_1 = 1.05c_2$, where c_1 and c_2 are the acoustic velocities of the medium outside the circle and inside the circle respectively. Also two simple models, for each of the linear and curved sequential array types of a foetus' head without a skull are created and display promising results which are not too dissimilar from images seen from scans of the BPD.

Finally, Chapter 5 presents two types of model which could provide a platform for quantifying US image distortion of a cross-section of a foetal head in-vivo. The model pertaining to the linear sequential array is given parameters relating to data for the properties of a foetus' head. Properties of the foetal skull are approximated in Section 2.5 and included in the linear model. Foetal images for a linear sequential array type are limited, due to the physical limitations of the transducer, so the focus of Chapter 5 is based upon the curved sequential array. The idea that he model could estimate the unknown properties of the skull is proposed and briefly explored.

As discussed in Chapter 2, artifacts can be produced if incorrect assumptions about the US beam's behaviour are made. All the models presented in this report presume that the US beam travels as a series of separate rays. As well as subjecting the models to rigorous tests to check their accuracy, a different type of the model could be developed using the properties of a wave, including solutions to the wave equation at boundaries between media. A model based on waves could model artifacts arising from attenuation, diffraction and even model the strength of the echoes.

Without invasive surgery, it is difficult to obtain the exact measurements of a particular foetus in-vivo. Knowledge of the exact dimensions of a particular foetus would be invaluable when developing a model to quantify the distortions. An experiment could be set up which would mimic the conditions of a foetus in-vivo. An ellipsoidal shell test object with the acoustic properties of a foetal skull could be imaged within a fluid, similar to the conditions within the womb and maintained at body temperature. The exact dimensions of the foetal skull model will be known and the distortions produced in the image could be accurately quantified and compared with theoretical predictions.

A contemporary problem within cross-disciplinary research, which includes mathematics, is the solution to the inverse problem. That is, if an image has been obtained, what is the structure of the object that caused it. In theory this sounds like a relatively simple problem, if the shape of the object and the acoustic velocities of all the media are approximately known, then a method similar to the one used in Chapter 5 could just be applied in reverse. Unfortunately in practice a point from an image has many possible points it could be mapped to, making this area of further research intricate and complex. However, should the inverse problem be solvable, the applications would be invaluable within medical diagnostics.

References

[1] A. Goldstein, "The effect of acoustic velocity on phantom measurements," *Ultrasound in Medicine & Biology*, vol. 26, no. 7, pp. 1133 – 1143, 2000.

[2] "Ovarian epithelial, fallopian tube, and primary peritoneal cancer treatment." `http://www.cancer.gov/cancertopics/pdq/treatment/ovarianepithelial/Patient/page1`, April 2015.

[3] "Obstetric ultrasound." `http://www.radiologyinfo.org/en/photocat/gallery3.cfm?image=baby-ultrasound.jpg&pg=obstetricus`, 2015.

[4] S. Dijkgraaf, "Spallanzani's unpublished experiments on the sensory basis of object perception in bats," *Isis*, vol. 51, pp. 9–20, March 1960.

[5] "Obstetric ultrasound." `http://www.cityofjoliet.com/halloffame/scientists/wnbeck.htm`, 2015.

[6] M. Felman, S. Katyal, and M. Blackwood, *US Artifacts*.

[7] "Wave rarefaction: Definition, curves & quiz." `http://study.com/academy/lesson/wave-rarefaction-definition-curves-quiz.html`, 2013.

[8] IRCAM, "Waveform introduction." `http://support.ircam.fr/docs/AudioSculpt/3.0/co/Acoustic20Notions.html`, 2011.

[9] "Manual of diagnostic ultrasound," *World Health Organization*, 2011.

[10] F. Duck, *Physical Properties of Tissue: A Comprehensive Reference Book*. 1990.

[11] P. Wells Distinguished Research Professor, Cardiff School of Engineering, April 2015.

[12] "Obstetric ultrasound." `http://www.radiologyinfo.org/en/info.cfm?pg=genus#part_nine`, 2015.

[13] "Ultrasound exams." `http://www.meriter.com/services/medical-imaging-services/ultrasound-exams`, 2015.

[14] "Transducer arrays."
`http://www.examrefresh.com/transducer-arrays/`, 2015. Visual and audio material.

[15] P. Chan, Vincent and Anahi, "Basics of ultrasound imaging," in *Atlas of Ultrasound-Guided Procedures in Interventional Pain Management*, pp. 13–19, Springer, 2011.

[16] "Vietnamese medic ultrasound."
`http://www.ultrasoundmedicvn.com/2012/12/case-157-thyroid-cyst-with-comet-tail.html`, Dec 2012. Blog.

[17] "Basic physics of ultrasound and the dobbler effect," March 2015.

[18] "Principles of ob-gyn sonography."
`https://iame.com/online/principles_of_obgyn_sonography/content.php`, 2014.

[19] "Computer aided instruction."
`http://cai.md.chula.ac.th/lesson/lesson4417/content/w7_9.html`.

[20] "Ultrasound scanfetal growth scan."
`http://brochures.mater.org.au/Home/Brochures/Mater-Mothers-Hospital/Ultrasound-scan-fetal-growth-scan`, July 2014.

[21] S. Robson Consultant in Fetal Medicine, Newcastle upon Tyne Hospitals NHS Foundation Trust, March 2015.

[22] T. C. W. M. McDevitt, H. and S. Ahmed, "Quantitative ultrasound assessment of bone in preterm and term neonates," *Archives of Disease in Childhood-Fetal and Neonatal Edition*, vol. 90, no. 4, pp. F341–FF342, 2005.

[23] N. K. Snijders, R.J.M., "Fetal biometry at 14–40 weeks' gestation," *Ultrasound in Obstetrics & Gynecology*, vol. 4, no. 1, pp. 34–48, 1994.